Citation for published version:
Dale, SEC, Vuorema, A, Sillanpää, M, Weber, J, Wain, AJ, Barnes, EO, Compton, RG & Marken, F 2014, 'Nano-litre proton/hydrogen titration in a dual-plate platinum-platinum generator-collector electrode micro-trench', *Electrochimica Acta*, vol. 125, pp. 94-100. https://doi.org/10.1016/j.electacta.2014.01.043

DOI:
10.1016/j.electacta.2014.01.043

Publication date:
2014

Document Version
Peer reviewed version

Link to publication

University of Bath

Alternative formats
If you require this document in an alternative format, please contact:
openaccess@bath.ac.uk

General rights
Copyright and moral rights for the publications made accessible in the public portal are retained by the authors and/or other copyright owners and it is a condition of accessing publications that users recognise and abide by the legal requirements associated with these rights.

Take down policy
If you believe that this document breaches copyright please contact us providing details, and we will remove access to the work immediately and investigate your claim.

Download date: 19. Mar. 2025

Revision

6th January 2014

Nano-Litre Proton/Hydrogen Titration in a Dual-Plate Platinum-Platinum Generator-Collector Electrode Micro-Trench

---

Sara E.C. Dale [a*], Anne Vuorema [b], Mika Sillanpää [b], James Weber [a], Andrew J. Wain [c], Edward O. Barnes [d], Richard G. Compton [d], and Frank Marken [a*]

[a] *Department of Chemistry, University of Bath, Bath BA2 7AY, UK*
[b] *Laboratory of Green Chemistry, Faculty of Technology, Lappeenranta University of Technology, Sammonkatu 12, FI-50130 Mikkeli, Finland*
[c] *National Physical Laboratory, Teddington, United Kingdom, TW11 0LW, UK*
[d] *Department of Chemistry, Physical and Theoretical Chemistry Laboratory, Oxford University, South Parks Road, Oxford OX1 3QZ, UK*

To be submitted to Electrochimica Acta

Proofs to Sara E.C. Dale

S.Dale@bath.ac.uk

Abstract

A generator-collector “nano-litre cavity” based on two opposed platinum-coated gold film electrodes with 19 μm gap and either 38 μm or 83 μm depth is employed for the titration of protons and/or hydrogen. Diffusional feedback currents between generator and collector electrode in a platinum-platinum dual-plate sensor configuration provide a sensitive analytical tool for cycleable redox systems, here, the proton/hydrogen redox system in the presence of oxygen.

Experimental data are compared with the theoretical expression proposed by Hubbard and Peters (A.T. Hubbard, D.G. Peters, Critical Reviews in Analytical Chemistry, 1973, 3, 201-242) suggesting a dominating transport effect of “slow diffusers”. Good agreement is observed even at relatively high proton concentrations where hydrogen bubble nucleation within the micro-trench starts to occur. Low concentration measurements are strongly affected by oxygen reduction locally consuming/depleting protons. Catalytic activity of the platinum deposit is crucial for maximising the current output.

Keywords: titration, hydrogen, micro-trench, electroanalysis, sensors.

1. Introduction

Proton titration is one of the most common and important analytical tasks [1] to be performed accurately and often in small volume. Amperometric methods have been developed [2,3,4,5,6] to complement measurements in complex media (e.g. containing colloids or proteins) where conventional glass-electrode potentiometry is less reliable. Thin layer electroanalytical methods [7] have been pioneered by Reilley [8] and Anson [9] and developed into analytical tools in particular for flow through sensors [10]. When combined with bipotentiostatic control (four-electrode control) generator-collector "feedback titrations" with dynamic endpoint are possible [11]. Generator-collector experiments were demonstrated for example by Bard *et al*. through the use of closely spaced ultramicroelectrodes [12]. Here the feasibility of proton/hydrogen determination in generator-collector feedback mode is investigated.

Nano-gap sensors [13,14] and junction sensors [15] have emerged recently for bipotentiostatic operation to provide amplified current responses for a range of analytes [16,17,18]. Improved analytical performance is observed with dual-plate generator-collector trench electrode systems [19] where a relatively uniform diffusion field exists over an extended area. Recently, pioneering work on nano-gap electrode systems produced via lithography has been reported by Lemay and coworkers [20] to provide access to extremely low detection limits theoretically approaching the single molecule level [21]. Therefore, chemical processes in dual-plate sensing devices are of considerable interest and potentially of wider applicability.

Hydrogen gas has many applications such as in the automobile industry [22], in operating fuel cell systems [23], in biological [24] and medical applications [25]. Hydrogen gas exhibits high diffusivity and permeability through many materials [26]. Hydrogen sensing by electrochemical means has been developed for many years [27]. Recently it has been shown that fast hydrogen gas sensing could be achieved with electrochemical micro-sensors [28,29] or when utilizing a gas-salt-electrode contact triple phase boundary system [30]. A palladium catalyst was immobilized on a glassy carbon electrode surface and placed in contact to solid ammonium sulfate and hydrogen gas. In this study the proton/hydrogen redox system is used as a model sensor system to explore the reactivity in a platinum-platinum dual-plate micro-trench sensor with protons and H_2 providing a case of unequal diffusivities.

Chemically, the hydrogen evolution reaction or the hydrogen oxidation are well-known and studied processes which occur readily (reversibly) on platinum electrodes [31]. In acidic aqueous solution and on platinum, the process is thought to be dominated by the Heyrovsky reaction step [32,33,34] in a two-step mechanism (see equations 1 and 2).

$$H^+ + e^- \rightarrow H_{ads} \quad (1)$$

$$H_{ads} + H^+ + e^- \rightarrow H_2 \quad (2)$$

In the present paper, platinum electro-plating is employed to fabricate a novel platinum-platinum dual-plate micro-trench sensor. Island platinum deposits on a gold substrate (see Figure 1) are formed and then employed in dual-plate configuration for

hydrogen sensing. This process can be understood as a “nano-litre” titration with dynamic endpoint.

2. Experimental

2.1. Chemical Reagents

Potassium ferricyanide, potassium hexachloroplatinate(IV), di-sodium sulphate, nitric acid, hydrochloric acid, and hydrogen peroxide were purchased from Sigma-Aldrich and were used as received. Sulphuric acid and potassium chloride were obtained from Merck. Solutions were made with ultra-pure water (SG Ultra Clear^{TM}) with a resistivity of not less than 18.2 MΩ cm at 25 ^{o}C. Hydrogen gas was obtained from BOC. Experiments were carried out at room temperature 22 ± 2 ^{o}C.

2.2. Instrumentation and Micro-Trench Sensor Fabrication

Electrochemical measurements were carried out using a four electrode configuration with KCl-saturated calomel reference electrode (SCE, Radiometer), platinum wire counter electrode (CH Instruments), and two working electrodes (the platinum-platinum dual-plate electrode). Experiments were performed using a PGSTAT 12 bipotentiostat (Autolab, Metrohm, Netherlands).

The platinum-platinum dual-plate electrode was fabricated by first taking a gold coated microscope slide (100 nm gold coating with a titanium adhesion layer, Sigma-Aldrich, UK) and cutting it into slides of ca. 1 cm × 3 cm using a diamond cutter (Buehler Isomet 1000 precision saw, UK). A central 0.5 cm strip of the slides was isolated with Kapton tape (Farnell, UK) and the slides placed in an aqua regia solution

(1:3 v/v HNO_3:HCl) for 3 minutes to etch gold from the sides of the slides. The Kapton tape was then removed leaving a 0.5 cm × 3 cm strip of gold down the centre of the slide. Slides were then placed in a furnace at 500 ^oC for 30 minutes to oxidise the remaining titanium adhesion layer along the sides of the remaining gold strip, which were exposed during etching. The resistance of the exposed titanium adhesion layer was measured using a multimeter to check that the titanium layer was oxidised and not conducting. Platinum was electrodeposited onto the gold layer by dipping the end of the slides into a solution of 2 mM potassium hexachloroplatinate(IV) in 0.1 M sulphuric acid with a potential of 0.1 V (vs. SCE) applied to the slide for 900 seconds. This yielded a visible platinum layer on top of the gold. Slides were then stuck together with epoxy (SP106 multipurpose epoxy system, SP Gurit; two part epoxy was mixed together and left for 90 minutes before sticking slides together to avoid short circuiting of the two electrodes and to control the inter-electrode distance) and placed in a home-made press overnight for final curing. The end of the electrode was then sliced off with the diamond cutter and polished flat with polishing paper (silicon carbide paper, P320, P600, Buehler). To create the micro-trench between the two platinum plates, the end of the electrode was placed in Piranha solution (1:5 v/v H_2O_2:H_2SO_4) and sonicated for 5 minutes to etch out the epoxy (*Warning: Piranha solution is highly corrosive and appropriate precautions are needed*).

FIGURE 1

Figure 1 shows the electron microscopy image of the resulting micro-trench with a 19 μm gap and some platinum island growth on a 100 nm thick gold film visible in the trench interior. The end of the electrode, with the opening to the trench, was placed

into a cell with solution containing the redox system of interest. Capillary action allowed the trench to be filled without problems.

3. Theory

In order to describe the general case of feedback currents for redox systems with $D_{ox} \neq D_{red}$ in a dual-plate electrode system the approach by Hubbard and Peters is followed [35]. The case of four-electrode control for two infinite dual-plate electrodes with separation δ is derived here for the hydrogen evolution process (see equation 3).

$$2\ H^+(aq) + 2\ e^- \rightleftharpoons H_2(aq) \qquad (3)$$

For this process the average bulk concentration (or "total hydrogen") can be defined as $c_0 = 2c_{H_2} + c_{H^+}$. Due to the difference in diffusion coefficients D_{H^+} and D_{H_2}, c_0 may vary relative to the position between the two electrodes within the micro-trench (see Figure 2).

FIGURE 2

Starting from Fick's 2nd law for steady state (equation 4 [36]), double-integration provides access to the corresponding concentration gradients (equation 5A and 5B).

$$0 = D_{H^+} \frac{\partial^2 c_{H^+}}{\partial x^2} \qquad (4A) \qquad\qquad 0 = D_{H_2} \frac{\partial^2 c_{H_2}}{\partial x^2} \qquad (4B)$$

$$c_{H^+} = Ax + B \qquad (5A) \qquad\qquad c_{H_2} = A'x + B' \qquad (5B)$$

With appropriate boundary conditions at x = 0 (oxidation), $c_{H^+} = c^*_{H^+} = B$ and $c_{H_2} = 0 = B'$, and at $x = \delta$ (reduction), $c_{H^+} = 0 = A\delta + c^*_{H^+}$ and $c_{H_2} = c^*_{H_2} = A'\delta$, (here A, A', B, B' are constants) we obtain equation 6A and 6B with starred concentration indicating surface concentrations.

$$c_{H^+} = -\frac{c^*_{H^+}}{\delta}x + c^*_{H^+} \qquad (6A) \qquad\qquad c_{H_2} = \frac{c^*_{H_2}}{\delta}x \qquad (6B)$$

That is, linear concentration profiles are expected (see Figure 2) with coupled current fluxes according to equation 7.

$$2D_{H_2}\frac{c^*_{H_2}}{\delta} = D_{H^+}\frac{c^*_{H^+}}{\delta} \qquad (7)$$

It is now possible to compare the bulk concentration and the average concentration in the inter-electrode space $c_0 = c_{average} = 2c_{H_2} + c_{H^+}$ with $c_{average}$ given in equation 8.

$$c_0 = c_{average} = \frac{1}{\delta}\int_0^{\delta}[2\frac{c^*_{H_2}}{\delta}x - \frac{c^*_{H^+}}{\delta}x + c^*_{H^+}]dx = c^*_{H_2} + \frac{1}{2}c^*_{H^+} \qquad (8)$$

The resulting expression combined with equation 7 gives the interfacial concentrations $c^*_{H^+}$ and $c^*_{H_2}$ in equations 9 and 10, respectively.

$$c_0 = \frac{D_{H^+}}{2D_{H_2}} c^*_{H^+} + \frac{1}{2} c^*_{H^+} \quad \text{or} \quad c^*_{H^+} = 2c_0 \left(\frac{1}{1 + \frac{D_{H^+}}{D_{H_2}}} \right) \tag{9}$$

$$c_0 = c^*_{H_2} + \frac{D_{H_2}}{D_{H^+}} c^*_{H_2} \quad \text{or} \quad c^*_{H_2} = c_0 \left(\frac{1}{1 + \frac{D_{H_2}}{D_{H^+}}} \right) \tag{10}$$

The current under steady state conditions is obtained (consistent with literature reports [33]) from the corresponding fluxes as shown in equation 11. The corresponding general equation for a redox system with $c_0 = c_{red} + c_{ox}$ and diffusion coefficients D_{ox} and D_{red} is given in equation 12.

$$I_{lim} = \frac{2FAD_{H_2} c^*_{H_2}}{\delta} = \frac{FAD_{H^+} c^*_{H^+}}{\delta} = \frac{2FAc_0}{\delta} \frac{D_{H_2} \times D_{H^+}}{D_{H_2} + D_{H^+}} \tag{11}$$

$$I_{lim} = \frac{2FAc_0}{\delta} \frac{D_{red} \times D_{ox}}{D_{red} + D_{ox}} \tag{12}$$

In the case of equal diffusion coefficients the familiar Nernst layer expression (equation 13) is recovered [37].

$$I_{\text{lim}} = \frac{FADc_0}{\delta} \qquad (13)$$

4. Results and Discussion

4.1. Dual-Plate Micro-Trench Sensor Calibration

Geometry calibration of the platinum-platinum dual-plate electrode was carried out with 1 mM potassium ferrocyanide in aqueous 0.1 M KCl to obtain the electrode area and trench depth. Figure 3 shows cyclic voltammograms for the oxidation of ferrocyanide at the generator electrode accompanied by reduction at the collector with a midpoint potential of ca. 0.18 V vs. SCE (with the collector potential held at −0.2 V vs. SCE). Collector responses are close to constant up to 200 mVs^{-1} where the hysteresis parameter ΔE_H = 0.03 V (see Figure 3). For this one-electron redox system and assuming at least approximately $D_{ox} = D_{red}$, the gap between the two platinum plate electrodes can be estimated using the equation $\Delta E_H = 0.0071 \times \nu\delta^2 F/(DRT)$ [38] (where ΔE_H is the potential difference at half the collector current, ν is the scan rate, δ is the inter-electrode gap, F is Faraday's constant, D is the diffusion coefficient 7.26 × 10^{-10} m^2s^{-1} [39], R is the gas constant, and T is the absolute temperature). The estimated gap size was calculated as 20 μm, in good agreement with the SEM image shown in Figure 1.

FIGURE 3

Next, the electrode area and trench depth are obtained using equation 12 (*vide supra*) with I_{lim} = −0.7 μA as the collector limiting current (other parameters are n = 1, D_{ox} and D_{red} are the diffusion coefficients for $K_4Fe(CN)_6$ with D_{red} = 6.67 × 10^{-10} m^2s^{-1} and for $K_3Fe(CN)_6$ is D_{ox} = 7.26 × 10^{-10} m^2s^{-1} [37], A is the electrode area, c_o is the concentration of ferrocyanide (1 mM), and δ is the inter-electrode gap). The electrode area (= width × depth) is obtained as 1.9 × 10^{-7} m^2 and with a 5 mm width the trench depth is estimated to be ca. 38 μm. The volume of the solution within the gap can be calculated from the area of the electrode and the gap between the two electrodes which was calculated to be 3.8 × 10^{-12} m^3. The collection efficiency (= collector limiting current / generator limiting current) is typically 80% (see Figure 3) consistent with a relatively low aspect ratio of trench depth/inter-electrode gap ≈ 2. With additional Piranha etching the trench was deepened (not shown) to 83 μm depth and with the resulting collection efficiency approaching 100%.

4.2. Dual-Plate Micro-Trench Sensor Response to Protons

For the H^+/H_2 redox system in aqueous media the diffusion coefficients have been reported as D_{H^+} = 7.9 × 10^{-9} m^2s^{-1} and D_{H_2} = 4.5 × 10^{-9} m^2s^{-1} [40,41]. The platinum-platinum dual-plate electrode was first placed in a solution of 20 mM H_2SO_4 in Na_2SO_4 or in 0.5 M H_2SO_4 (see Figure 4A and B, respectively) to determine the effectiveness of the platinum coating.

FIGURE 4

Figure 4A shows cyclic voltammograms for the reduction of 20 mM H_2SO_4 in generator-collector mode and with the collector potential held at 0.5 V vs. SCE. The effect of changing the scan rate on the reduction and oxidation processes are clearly observed. Well-defined steady state limiting currents are observed with collection efficiency close to 100 %. At very high scan rates, 2 Vs^{-1}, two additional peaks could be seen on the generator signal (ca. −0.13 V and −0.25 V vs. SCE) corresponding to well-known underpotential deposition of hydrogen on platinum. The peak at −0.13 V vs. SCE is due to weak adsorption of hydrogen to the platinum surface and the peak at −0.25 V vs. SCE strong adsorption of hydrogen [42]. These peaks are not apparent in the collector current or visible for the generator electrode at slower scan rates because of their surface-confined nature. As the scan rate increases, the hysteresis effect in the collector current trace also increases indicating the lag time of the diffusion between the two electrodes. However, the hysteresis parameter ΔE_H is here significantly higher compared to that expected for a 19 μm inter-electrode gap (*vide supra*) possibly due to additional effects from hydrogen bubbles.

Figure 4B shows a generator-collector cyclic voltammogram obtained in 0.5 M H_2SO_4 and with the collector potential held at 0.5 V vs. SCE. At approximately −0.3 V vs. SCE, there is a sharp increase in current indicating the reduction of protons at the generator and oxidation of H_2 and the collector electrode. Perhaps surprisingly, the collector current initially increases but then stagnates with additional noise indicating the formation of H_2 gas bubbles within the micro-trench (see drawing in inset in Figure 4B).

FIGURE 5

A more detailed study of the effect of proton concentration is shown in Figure 5. Non-ideal behaviour is apparent in particular at high proton concentration (due to hydrogen bubble formation; see Figure 5Axiii) and at low concentration (see Figure 5B) where the limiting currents for the negative going and the positive going potential scans are non-equal (here probably due to changes in catalyst activity, that is non-sufficient catalyst activity for reaching mass transport limited conditions). Although a clear monotonic change of limiting current with proton concentration is observed (not shown) a double-logarithmic plot reveals deviation from ideal behaviour. A non-linearity at low proton concentrations is observed when plotting the current data versus concentration (see Figure 5C and D). The theory line based on equation 11 appears to generally over-estimate the currents (possibly due to a kinetic limit in platinum catalyst turn over) and in particular for concentrations of 1 mM H_2SO_4 and lower. This low concentration non-linearity can be shown to be due to oxygen interference. De-aerated solutions show close to linear dependency (not shown), although even low level residual oxygen causes deviation in the lower proton concentration range. Due to the chemically irreversible nature of the oxygen reduction reaction to hydroxide (in the trench mouth region), protons in the micro-trench region are consumed [43]. This causes a competing flux of oxygen and protons towards the micro-trench "mouth" region and a significant decrease in the H^+/H_2 feedback current. When using the approximate equation for the mass transport limited current at a micro-band electrode [44], which describes diffusional flux from open solution to the inter-electrode zone, it is possible to estimate this effect of oxygen flux on the

apparent or remaining proton concentration within the micro-trench interior (equation 14).

$$c_{H^+,interior} = c_{H^+,bulk} - \Delta c_{H^+} = c_{H^+,bulk} - 4\frac{D_{O_2}}{D_{H^+}}\frac{\ln\left(\frac{8\sqrt{D_{H^+}t}}{w}\right)}{\ln\left(\frac{8\sqrt{D_{O_2}t}}{w}\right)}c_{O_2,bulk} \qquad (14)$$

In this equation (w is the trench width with a corresponding diffusional flux to the "microgap") the logarithmic terms of this type cancel out at high time t. A pale grey line (see line (ii) in Figure 5C and 5D) shows the approximate effect of ambient levels of oxygen in solution introducing a curvature consistent with that observed for the experimental data.

Hydrogen bubble formation (which should occur for concentrations of 0.6 mM H_2SO_4 and higher [45]) has a surprisingly small effect on the linearity of the limiting current plots. Equation 11 seems to remain approximately valid over an extended concentration range, which can be explained (at least in part) based on supersaturation effects or slow bubble nucleation and growth rates. Further improvements in the low-concentration linearity are possible with oxygen exclusion during measurements (*vide supra*).

FIGURE 6

Chronoamperometry experiments were carried out in order to explore the time-dependence of generator and collector currents. Figure 6A shows data for the reduction of 2.5 mM H_2SO_4. A considerable mismatch of generator and collector currents is indicative of additional oxygen reduction. A rising collector current is observed consistent with a diffusional delay across the inter-electrode gap. In contrast, data for a 20 mM H_2SO_4 shows an initial current peak for both generator and collector electrode followed by a "noisy" decay. This is consistent with a hydrogen bubble development affecting mass transport in the early stages of the process.

4.3. Dual-Plate Micro-Trench Sensor Response to Hydrogen

Platinum-platinum dual-plate electrodes are responsive for the H^+/H_2 redox system and could therefore be applied also to hydrogen gas sensing (see equation 11). Here, hydrogen gas is bubbled through a solution of 20 mM H_2SO_4 and 0.5 M Na_2SO_4 and the generator-collector current measured in feedback mode. Figure 7 shows the cyclic voltammogram for the platinum-platinum dual-plate electrode both with and without hydrogen gas bubbled through the solution. There is a clear increase in current on both the generator and collector when hydrogen gas has been bubbled through the solution compared to when no hydrogen gas was used. Based on the expression $c_0 = 2c_{H_2} + c_{H^+}$ and assuming ca. 0.6 mM to 0.8 mM H_2 dissolved in the solution [46], c_0 should increase from 40 mM to 41.2 mM. The significant additional increase observed here could be associated with (i) changes in hydrogen bubble dynamics and effects in the micro-trench and (ii) additional oxygen removal effects.

FIGURE 7

Finally, when hydrogen is pre-saturated into a solution of 0.5 M Na_2SO_4 in the absence of a significant bulk concentration of protons, the oxidation of hydrogen in the Pt-Pt micro-trench is observed directly (see Figure 7B). In this case the parameter $c_0 = 2c_{H_2} + c_{H^+}$ should be approximately 1.2 mM, which is in the non-linear region of the plot in Figure 5C. Therefore, the observed mass transport limited current is affected by oxygen and when continuously cycling the potential (Figure 7C) a rapid loss of signal is apparent. For both, low concentration proton titration or dissolved hydrogen gas titration, trace oxygen needs to be eliminated as far as possible to allow the linear range of equation 11 to extend into the low concentration region. For mixed solutions containing protons and hydrogen the relative amounts are not directly accessible from the Pt-Pt dual-plate micro-trench limiting currents. The additional determination of the equilibrium potential could be employed to overcome this problem.

5. Summary and Conclusions

The Pt-Pt micro-trench electrode is a useful electroanalytical tool and with additional improvements in situ titration of proton/hydrogen concentration could be possible even in the presence of oxygen. The main results from this study are:

(i) The depth of the micro-trench can be adjusted (or the gap decreased) to optimise current readings and to increase amplification effects.

(ii) A good correlation of proton concentration to sensor response is observed even at high concentrations where hydrogen bubble formation in the micro-trench is likely to occur.

(iii) A poor sensor response to protons at low concentrations is due to severe "oxygen interference" and an improved oxygen exclusion could considerably increase the low concentration sensitivity of the micro-trench electrode.

(iv) For proton-hydrogen mixtures additional information such as the equilibrium potential is required in order to resolve relative concentrations.

(v) An important problem to resolve in future is the platinum catalyst activity which under the high mass transport conditions employed here is not sufficient. As a result the micro-trench sensor appears to exhibit a lower "apparent active area" and in the double logarithmic plot of limiting current versus concentration experimental limiting currents appears shifted downwards.

(vi) If catalytic activity can be improved, then decreasing the inter-electrode distance below the micro-meter range could provide a very interesting tool to further widen the measurement range into the higher and lower concentration domains.

Current feedback in generator-collector micro-trench sensors offers a chemically versatile and sensitive tool, for example to dissect complex chemical mixtures. One considerable benefit is the small volume required with only nano-litre space in the

micro-trench interior being active. The limiting current observed for a cycleable redox system reflects the bulk concentration without significantly depleting the bulk concentration. The process is therefore reminiscent of a nano-litre titration process with dynamic end point. However, for real applications, inter-electrode gap processes need to be better understood in terms of (i) catalyst activity, (ii) diffusional transport, (iii) concentration gradients, and (iv) associated chemical/physical reactions including bubble/solid nucleation and/or precipitation. In future, the fabrication of nano-trench electrodes will provide significant further improvements in miniaturisation and sensitivity.

Acknowledgements

S. E. C. D. and E. O. B. would like to thank the EPSRC for funding (EP/IO28706/1). J.W. and A.J.W acknowledge the financial support of the UK National Measurement System. The authors thank John M. Mitchels and Ursula Potter for assistance with electron microscopy. A.V. would like to thank the Academy of Finland for funding.

References

[1] K.H. Lubert, K. Kalcher, Electroanalysis 22 (2010) 1937-1946.

[2] C. Batchelor-McAuley, C.E. Banks, A.O. Simm, T.G.J. Jones, R.G. Compton, ChemPhysChem 7 (2006) 1081-1085.

[3] D.S. Silvester, L. Aldous, C. Hardacre, R.G. Compton, J. Phys. Chem. B 111 (2007) 5000-5007.

[4] D.S. Silvester, K.R. Ward, L. Aldous, C. Hardacre, R.G. Compton, J. Electroanal. Chem. 618 (2008) 53-60.

[5] Y. Meng, L. Aldous, R.G. Compton, J. Phys. Chem. C 115 (2011) 14334-14340.

[6] Y. Meng, L. Aldous, S.R. Belding, R.G. Compton, Chem. Commun. 48 (2012) 5572-5574.

[7] C.N. Reilley, Rev. Pure Appl. Chem. 18 (1968) 137.

[8] L.B. Anderson, C.N. Reilley, J. Electroanal. Chem. 10 (1965) 538.

[9] C.R. Christensen, F.C. Anson, Anal. Chem. 35 (1963) 205.

[10] Y.I. Turyan, Talanta 44 (1997) 1-13.

[11] H. Rajantie, J. Strutwolf, D.E. Williams, J. Electroanal. Chem. 500 (2001) 108-120.

[12] A. J. Bard, J. A. Crayston, G. P. Kittlesen, T. V. Shea, M. S. Wrighton, Anal. Chem. 58 (1986) 2321-2331.

[13] S.E.C. Dale, A. Vuorema, E.M.Y. Ashmore, B. Kasprzyk-Hordern, M. Sillanpää, G. Denuault, F. Marken, Chem. Record 12 (2012) 143-148.

[14] I.J. Cutress, Y. Wang, J.G. Limon-Petersen, S.E.C. Dale, L. Rassaei, R.G. Compton, J. Electroanal. Chem. 655 (2011) 147-153.

[15] E.O. Barnes, G.E.M. Lewis, S.E.C. Dale, F. Marken, R.G. Compton, Analyst 137 (2012) 1068-1081.

[16] G.E.M. Lewis, S.E.C. Dale, B. Kasprzyk-Hordern, E.O. Barnes, R.G. Compton, F. Marken, Electroanalysis 24 (2012) 1726-1731.

[17] S.E.C. Dale, Y. Chan, P.C. Bulman Page, E.O. Barnes, R.G. Compton, F. Marken, Electrophoresis 34 (2013) 1979-1984.

[18] L. Rassaei, F. Marken, Anal. Chem. 82 (2010) 7063-7067.

[19] S.E.C. Dale, C.E. Hotchen, F. Marken, Electrochim. Acta 101 (2013) 196-200.

[20] E. Katelhon, B. Hofmann, S. G. Lemay, M. A. G. Zevenbergen, A. Offenhausser, B. Wolfrum, Anal. Chem. 82 (2010) 8502-8509.

[21] M.A.G. Zevenbergen, P.S. Singh, E.D. Goluch, B.L. Wolfrum, S.G. Lemay, Nano Lett. 11 (2011) 2881-2886.

[22] J.H. Wee, Ren. Sustain. Energy Rev. 11 (2007) 1720-1738.

[23] L. Carrette, K. A. Friedrich, U. Stimming, Chem. Phys. Chem. 1 (2000) 162-193.

[24] P.C. Hallenbeck, J.R. Benemann, Int. J. Hydrogen Energy 27 (2002) 1185-1193.

[25] I. Ohsawa, M. Ishikawa, K. Takahshi, M. Watanabe, K. Nishimaki, K. Yamagata, K. Katsura, Y. Katayama, S. Asoh, S. Ohta, Nature Medicine 13 (2007) 688-694.

[26] N.W. Ockwig, T.M. Nenoff, Chem. Rev. 107 (2007) 4078-4110.

[27] G. Korotcenkov, S.D. Han, J.R. Stetter, Chem. Rev. (109) 2009 1402-1433.

[28] R.M. Penner, Ann. Rev. Anal. Chem. 5 (2012) 461-485.

[29] F. Yang, D. Jung, R.M. Penner, Anal. Chem. 83 (2011) 9472-9477.

[30] F. Xia, S.E.C. Dale, R.A. Webster, M. Pan, S. Mu, S.C. Tsang, J.M. Mitchels, F. Marken, New J. Chem. 35 (2011) 1855-1860.

[31] R. Parsons, Trans. Faraday Soc. 56 (1960) 1340-1350.

[32] P.H. Rieger, Electrochemistry, Prentice-Hall, Englewood Cliffs, London, 1987.

[33] L.A. Kibler, ChemPhysChem 7 (2006) 985–991.

[34] Y. Meng, L. Aldous, S.R. Belding, R.G. Compton, ChemPhysChem 14 (2012) 5222-5228.

[35] A.T. Hubbard, D.G. Peters, CRC Crit. Rev. Anal. Chem. 3 (1973) 201-242.

[36] A.J. Bard, L.R. Faulkner, Electrochemical Methods, Wiley, New York, 2001, p. 148.

[37] A.J. Bard, L.R. Faulkner, Electrochemical Methods, Wiley, New York, 2001, p. 29.

[38] R.W. French, F. Marken, J. Solid State Electrochem. 13 (2009) 609-617.

[39] S.J. Konopka, B. McDuffle, Anal. Chem. 42 (1970) 1741-1746.

[40] J.V. Macpherson, P.R. Unwin, Anal. Chem. 69 (1997) 2063-2069.

[41] D. Cavagnat, J.C. Lassegues, Solid State Ionics 46 (1991) 11-17.

[42] B. Losiewicz, R. Jurczakowksi, A. Lasia, Electrochim. Acta 80 (2012) 292-301.

[43] S.E.C. Dale, C.E. Hotchen, F. Marken, Electrochim. Acta 101 (2013) 196-200.

[44] C. Amatore, Physical Electrochemistry, I. Rubinstein (ed.), Marcel Dekker, New York, 1995, p. 151.

[45] K. Aoki, H. Toda, J. Yamamoto, J.Y. Chen, T. Nishiumi, J. Electroanal. Chem. 668 (2012) 83-89.

[46] W.F. Linke. Solubilities of Inorganic and Metal Organic Compounds, American Chemical Society, Washington DC, 1958, Vol. I, p. 1081.

Figure Captions:

Figure 1. (A) and (B) schematic drawing of the construction of the trench electrode. SEM images of the Pt-Pt dual-plate electrode gap with (C) low and (D) high magnification showing a 19 μm inter-electrode gap and platinum island deposits on a 100 nm thick gold film electrode.

Figure 2. Schematic drawing of (A) a trench electrode without applied potential and (B) a trench electrode under steady state conditions of a four-electrode potential control [33]. Concentration versus distance plots are indicated. The dashed black line indicates the case for $D_{red} = D_{ox}$ and the dashed red line indicates the case for $D_{red} < D_{ox}$ causing a build-up of c_{red} at the cathode.

Figure 3. Voltammetric signals (scan rate (i) 10, (ii) 20, (iii) 50, (iv) 100, (v) 200 mVs^{-1}) for a Pt-Pt dual-plate micro-trench electrode immersed in 1 mM potassium ferrocyanide / 0.1 M KCl with collector potential held at −0.2 V vs. SCE.

Figure 4. (A) Cyclic voltammograms (scan rate (i) 20, (ii) 50, (iii) 100, (iv) 200, (v) 500, (vi) 1000, and (vii) 2000 mVs^{-1}) for a Pt-Pt micro-trench electrode immersed in 20 mM H_2SO_4 / 0.5 M Na_2SO_4 with fixed collector electrode potential at 0.5 V vs. SCE. (B) Cyclic voltammogram (scan rate 20 mVs^{-1}) for a Pt-Pt micro-trench electrode immersed in 0.5 M H_2SO_4 with the collector electrode held at 0.5 V vs. SCE.

Figure 5. (A) Cyclic voltammograms (scan rate 20 mVs^{-1}) obtained at a Pt-Pt micro-trench (38 μm deep) for concentrations of (i) 0.0, (ii) 0.2, (iii) 0.4, (iv) 0.6, (v) 0.8, (vi) 1.0, (vii) 2.5, (viii) 5, (ix) 10, (x) 20, (xi) 40, (xii) 80, and (xiii) 160 mM H_2SO_4 with the collector electrode potential of 0.5 V vs. SCE. (B) As before with only (i) 0.4, (ii) 0.6, (iii) 0.8 mM H_2SO_4. (C) Plot of generator and collector current data as a

function of H_2SO_4 concentration for trench depth 38 μm. (D) As before but for trench depth 83 μm. A solid grey line (i) shows the theory based on equation 7 with a more pale line (ii) indicating the effect of oxygen.

Figure 6. (A) Chronoamperograms at Pt-Pt micro-trench electrodes with 38 μm depth immersed in 2.5 mM H_2SO_4/0.5 M Na_2SO_4. The generator electrode potential is stepped from 0.5 V to −0.8 V to 0.5 V vs. SCE and the collector electrode potential is held at 0.5 V vs. SCE. (B) As before but with 20 mM H_2SO_4 / 0.5 M Na_2SO_4.

Figure 7. (A) Cyclic voltammograms (scan rate 20 mVs^{-1}) for a Pt-Pt micro-trench electrode (38 μm deep) immersed in 20 mM H_2SO_4 / 0.5 M Na_2SO_4 with/without H_2 pre-saturation (collector electrode was held at 0.5 V vs. SCE). (B) As before, but for H_2 pre-saturated in 0.5 M Na_2SO_4 solution (collector electrode was held at -0.8 V vs. SCE). (C) As before, with continuous potential cycling.

Figures:

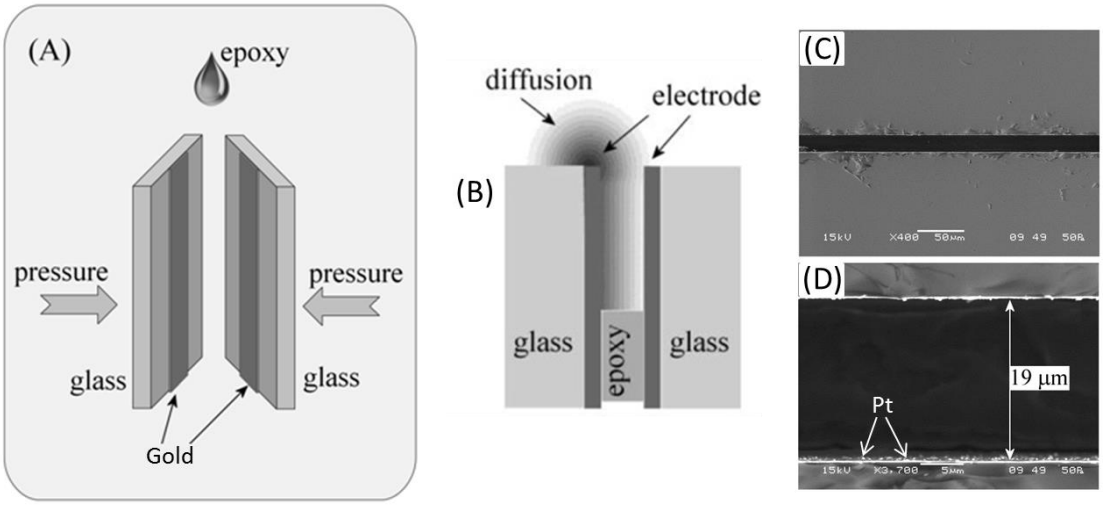

Figure 1. (A) and (B) schematic drawing of the construction of the trench electrode. SEM images of the Pt-Pt dual-plate electrode gap with (C) low and (D) high magnification showing a 19 µm inter-electrode gap and platinum island deposits on a 100 nm thick gold film electrode.

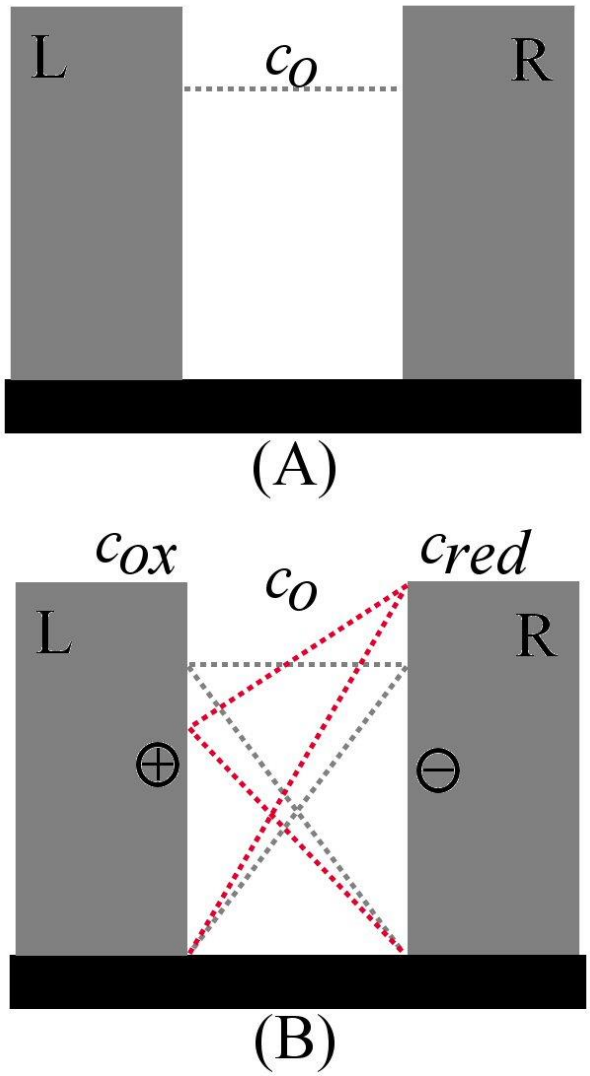

Figure 2. Schematic drawing of (A) a trench electrode without applied potential and (B) a trench electrode under steady state conditions of a four-electrode potential control [33]. Concentration versus distance plots are indicated. The dashed black line indicates the case for $D_{red} = D_{ox}$ and the dashed red line indicates the case for $D_{red} < D_{ox}$ causing a build-up of c_{red} at the cathode.

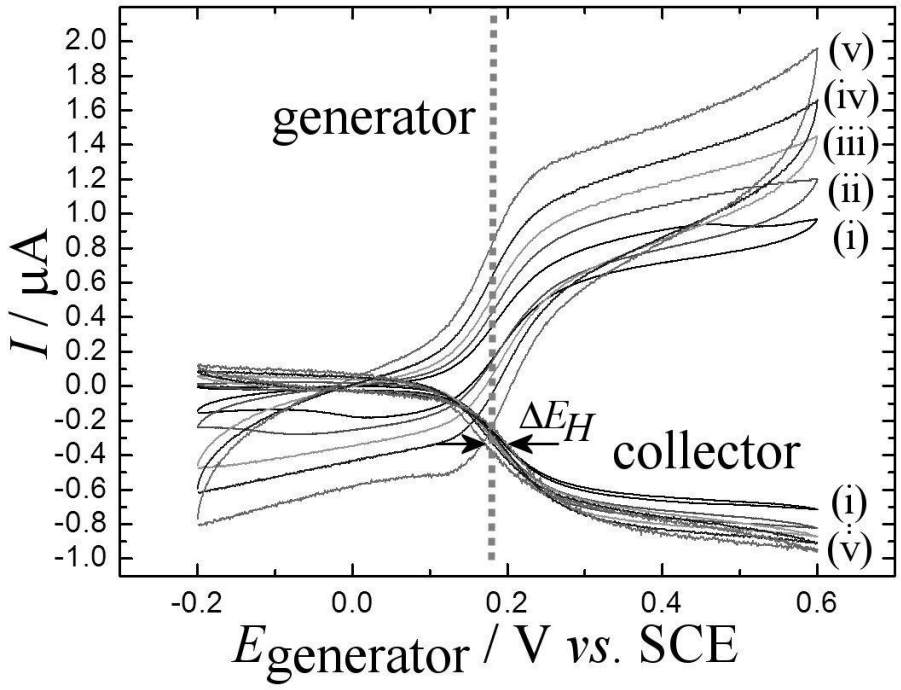

Figure 3. Voltammetric signals (scan rate (i) 10, (ii) 20, (iii) 50, (iv) 100, (v) 200 mVs^{-1}) for a Pt-Pt dual-plate micro-trench electrode immersed in 1 mM potassium ferrocyanide / 0.1 M KCl with collector potential held at −0.2 V vs. SCE.

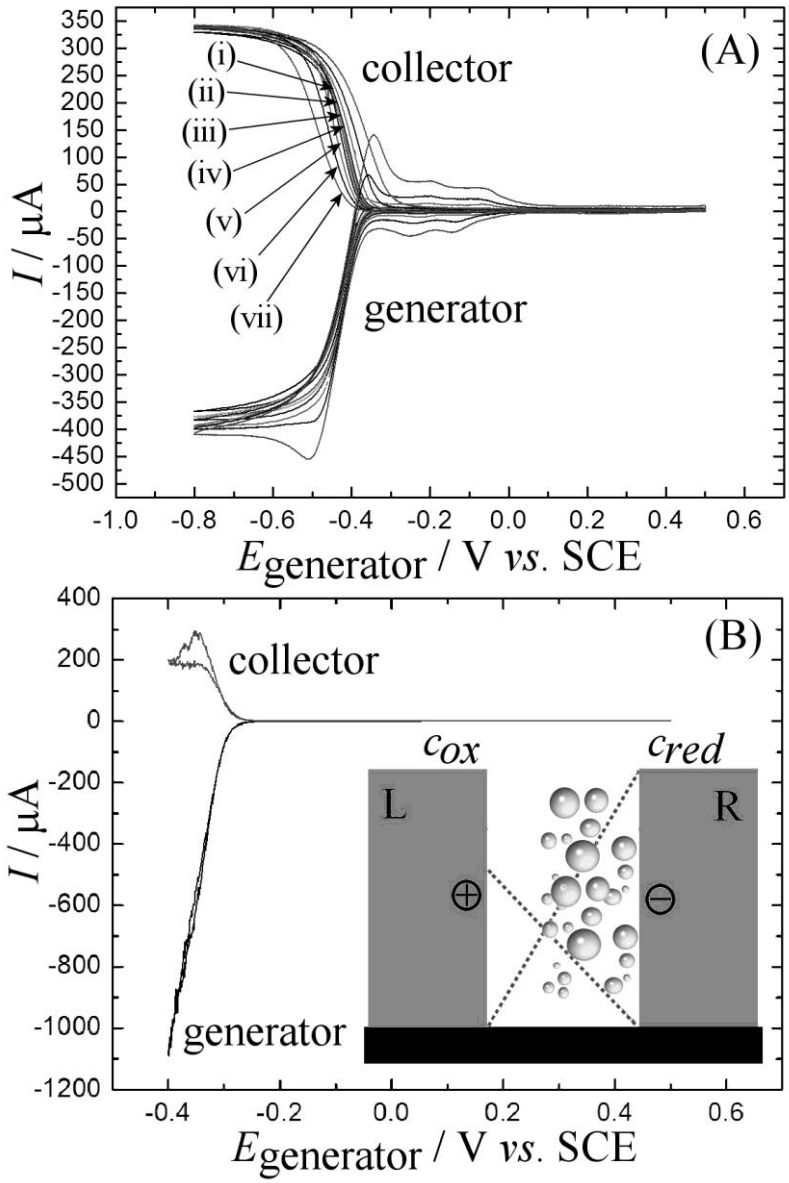

Figure 4. (A) Cyclic voltammograms (scan rate (i) 20, (ii) 50, (iii) 100, (iv) 200, (v) 500, (vi) 1000, and (vii) 2000 mVs^{-1}) for a Pt-Pt micro-trench electrode immersed in 20 mM H_2SO_4 / 0.5 M Na_2SO_4 with fixed collector electrode potential at 0.5 V vs. SCE. (B) Cyclic voltammogram (scan rate 20 mVs^{-1}) for a Pt-Pt micro-trench electrode immersed in 0.5 M H_2SO_4 with the collector electrode held at 0.5 V vs. SCE.

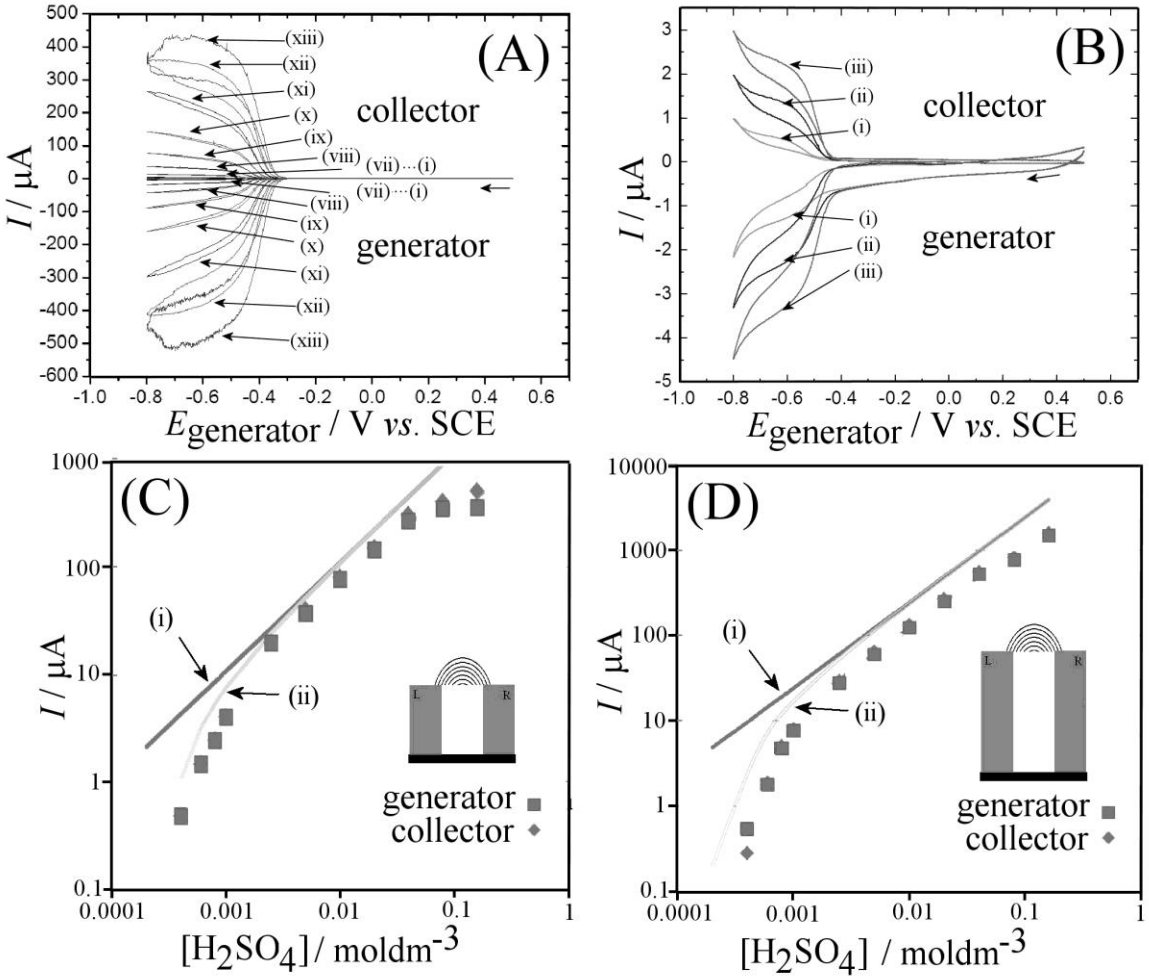

Figure 5. (A) Cyclic voltammograms (scan rate 20 mVs^{-1}) obtained at a Pt-Pt micro-trench (38 μm deep) for concentrations of (i) 0.0, (ii) 0.2, (iii) 0.4, (iv) 0.6, (v) 0.8, (vi) 1.0, (vii) 2.5, (viii) 5, (ix) 10, (x) 20, (xi) 40, (xii) 80, and (xiii) 160 mM H_2SO_4 with the collector electrode potential of 0.5 V vs. SCE. (B) As before with only (i) 0.4, (ii) 0.6, (iii) 0.8 mM H_2SO_4. (C) Plot of generator and collector current data as a function of H_2SO_4 concentration for trench depth 38 μm. (D) As before but for trench depth 83 μm. A solid grey line (i) shows the theory based on equation 7 with a more pale line (ii) indicating the effect of oxygen.

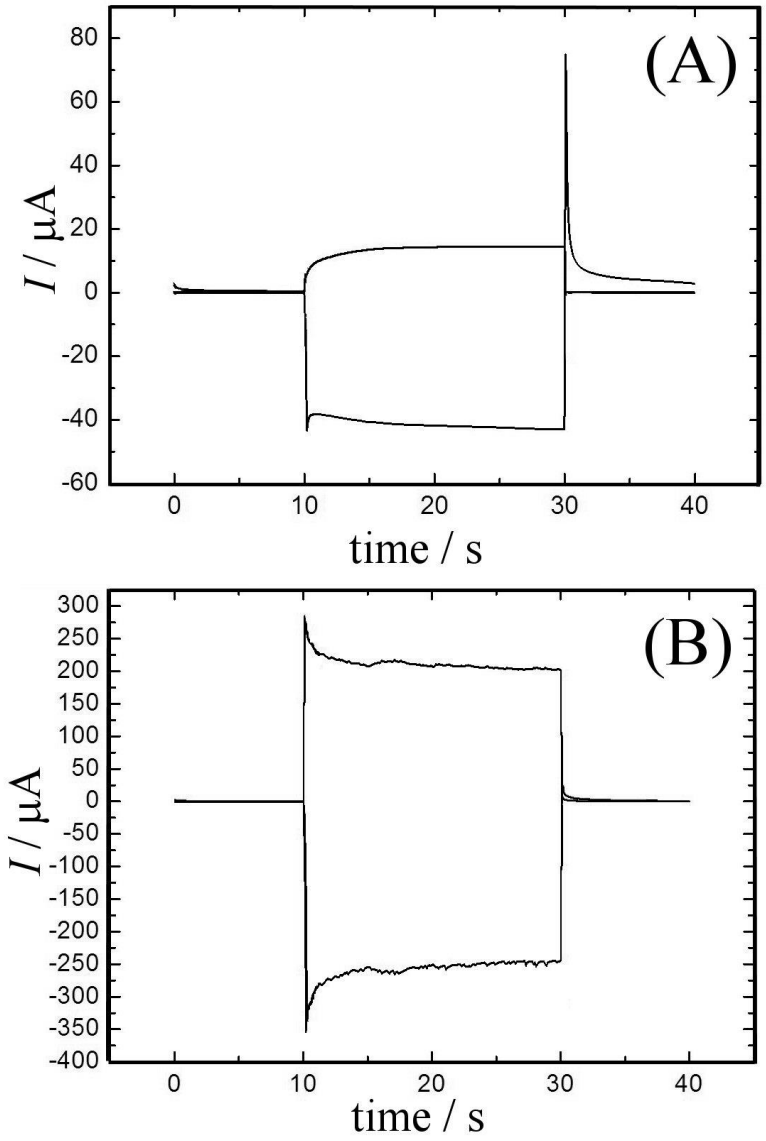

Figure 6. (A) Chronoamperograms at Pt-Pt micro-trench electrodes with 38 μm depth immersed in 2.5 mM H_2SO_4/0.5 M Na_2SO_4. The generator electrode potential is stepped from 0.5 V to −0.8 V to 0.5 V vs. SCE and the collector electrode potential is held at 0.5 V vs. SCE. (B) As before but with 20 mM H_2SO_4 / 0.5 M Na_2SO_4.

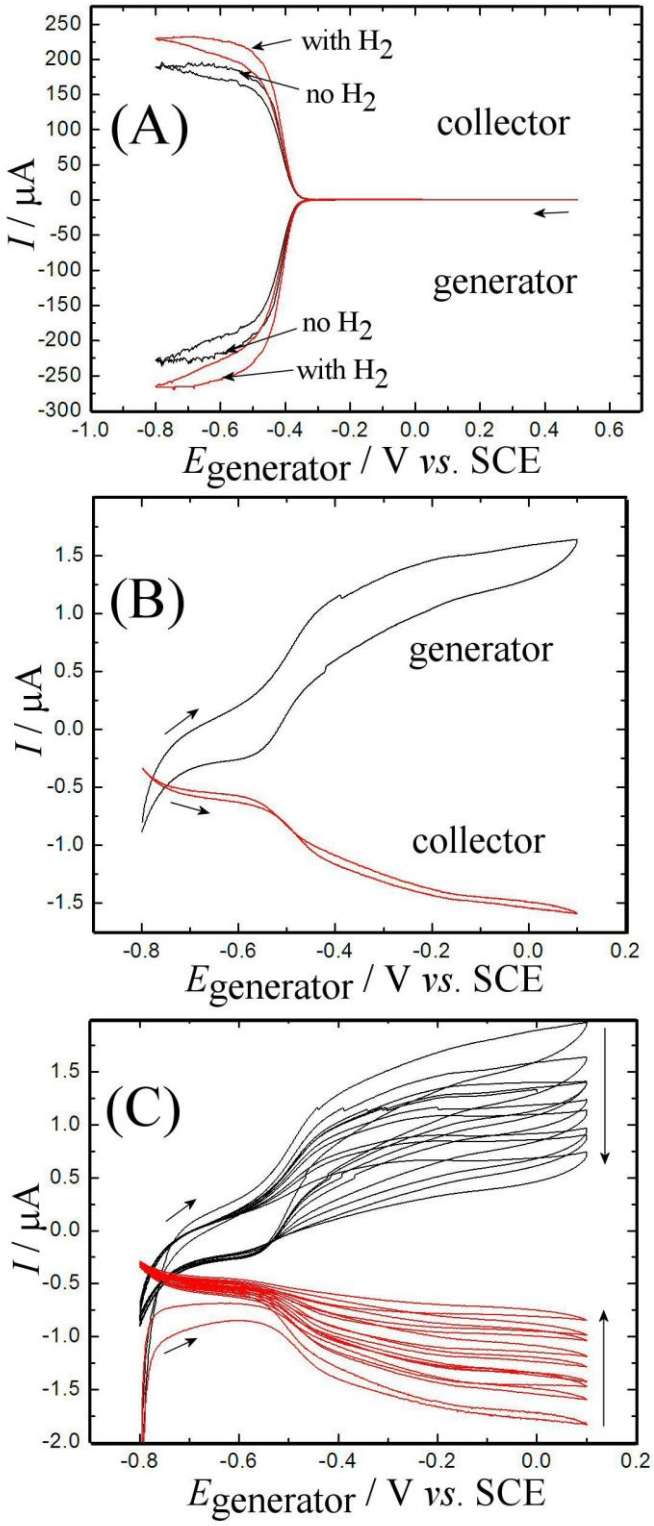

Figure 7. (A) Cyclic voltammograms (scan rate 20 mVs^{-1}) for a Pt-Pt micro-trench electrode (38 μm deep) immersed in 20 mM H_2SO_4 / 0.5 M Na_2SO_4 with/without H_2 pre-saturation (collector electrode was held at 0.5 V vs. SCE). (B) As before, but for H_2 pre-saturated in 0.5 M Na_2SO_4 solution (collector electrode was held at -0.8 V vs. SCE). (C) As before, with continuous potential cycling.